Airborne LiDAR analysis and geochronology of faulted glacial moraines in the Tahoe-Sierra frontal fault zone reveal substantial seismic hazards in the Lake Tahoe region, California-Nevada, USA

James F. Howle[1,†], Gerald W. Bawden[2,†], Richard A. Schweickert[3,†], Robert C. Finkel[4,†], Lewis E. Hunter[5,†], Ronn S. Rose[5,†], and Brent von Twistern[6,†]

[1]*U.S. Geological Survey, P.O. Box 1360, Carnelian Bay, California 96140, USA*
[2]*U.S. Geological Survey, 3020 State University Drive East, Modoc Hall, Suite 4004, Sacramento, California 95819, USA*
[3]*University of Nevada, Reno, Department of Geological Sciences, 1900 Greensburg Circle, Reno, Nevada 89509, USA*
[4]*University of California, Berkeley, Earth and Planetary Science Department, 371 McCone Hall, Berkeley, California 94720, USA*
[5]*U.S. Army Corp of Engineers, 1325 J Street, Sacramento, California 95814, USA*
[6]*P.O. Box 5401, Incline Village, Nevada 89450, USA*

ABSTRACT

We integrated high-resolution bare-earth airborne light detection and ranging (LiDAR) imagery with field observations and modern geochronology to characterize the Tahoe-Sierra frontal fault zone, which forms the neotectonic boundary between the Sierra Nevada and the Basin and Range Province west of Lake Tahoe. The LiDAR imagery clearly delineates active normal faults that have displaced late Pleistocene glacial moraines and Holocene alluvium along 30 km of linear, right-stepping range front of the Tahoe-Sierra frontal fault zone. Herein, we illustrate and describe the tectonic geomorphology of faulted lateral moraines. We have developed new, three-dimensional modeling techniques that utilize the high-resolution LiDAR data to determine tectonic displacements of moraine crests and alluvium. The statistically robust displacement models combined with new ages of the displaced Tioga (20.8 ± 1.4 ka) and Tahoe (69.2 ± 4.8 ka; 73.2 ± 8.7 ka) moraines are used to estimate the minimum vertical separation rate at 17 sites along the Tahoe-Sierra frontal fault zone. Near the northern end of the study area, the minimum vertical separation rate is 1.5 ± 0.4 mm/yr, which represents a two- to threefold increase in estimates of seismic moment for the Lake Tahoe basin. From this study, we conclude that potential earthquake moment magnitudes (M_w) range from 6.3 ± 0.25 to 6.9 ± 0.25. A close spatial association of landslides and active faults suggests that landslides have been seismically triggered. Our study underscores that the Tahoe-Sierra frontal fault zone poses substantial seismic and landslide hazards.

INTRODUCTION

The Lake Tahoe basin, California and Nevada, is a tectonically active graben located between the Sierra Nevada microplate on the west and the Basin and Range Province to the east. The Tahoe-Sierra frontal fault zone, west of Lake Tahoe, was recognized over a century ago by early geologic investigators (Russell, 1885; Lindgren, 1896, 1897) from its topographic expression, but the locations of basin-bounding normal faults have remained elusive due to difficult access and dense vegetative cover in mountainous terrain. Schweickert et al. (2000, 2004) mapped the principal faults of the Tahoe-Sierra frontal fault zone along the steep, linear range front west of the lake. However, because complex tectonic geomorphology has been formed by normal faulting of glacial landforms and because dense vegetation obscures the morphology, the fault zone has remained controversial and was omitted from the state of California's seismic hazard risk assessment (UCERF2, 2007). This report documents the tectonic geomorphology of faulted moraines, establishes limiting ages of faulted late Pleistocene glacial and alluvial deposits, and quantifies the minimum vertical separation rate and extension rate along the Tahoe-Sierra frontal fault zone; it demonstrates that the Tahoe-Sierra frontal fault zone is an important seismic source for the region.

Bare-earth airborne light detection and ranging (LiDAR) imagery has revolutionized geomorphic mapping in densely vegetated, mountainous, and otherwise inaccessible terrain (Fig. 1). Recent studies of known fault zones (Hudnut et al., 2002; Frankel et al., 2007; Oskin et al., 2007; Prentice et al., 2009; Arrowsmith and Zielke, 2009; Zielke et al., 2010) and discoveries of previously unknown fault zones in densely vegetated terrain (Haugerud et al., 2003; Hunter et al., 2011) have exploited bare-earth airborne LiDAR imagery for fault-zone characterization. Utilizing new bare-earth LiDAR imagery (see GSA Data Repository for a discussion of the LiDAR data used in this study[1]) we have identified, visualized, and mapped faults within late Quaternary glacial, colluvial, and alluvial deposits and granitic bedrock along 30 km of range-front faults that comprise the central portion of the Tahoe-Sierra frontal fault zone (Fig. 2). We analyzed the LiDAR imagery using pseudo–sun angles, vertical exaggeration, and oblique perspectives and extracted profiles to facilitate geologic interpretation and to reveal (and in many cases confirm)

†E-mails: jfhowle@usgs.gov; gbawden@usgs.gov; rschweickert@gmail.com; rfinkel@berkeley.edu; lewis.e.hunter@usace.army.mil; ronn.s.rose@usace.army.mil; bvtwist@journeyaroundhappy.com.

[1]GSA Data Repository item 2012192, includes supplementary discussions of the airborne LiDAR data, late Pleistocene glacial deposits and stratigraphy, geochronology of Tioga and Tahoe deposits, Emerald Bay bathymetric data, mathematical modeling of planes and vectors, Root-Mean-Square error estimates, modeled tectonic displacements, DR Figures 1–16 and DR Tables 1–6, is available at http://www.geosociety.org/pubs/ft2012.htm or by request to editing@geosociety.org.

GSA Bulletin; doi:10.1130/B30598.1; 8 figures; 1 table; Data Repository item 2012192.

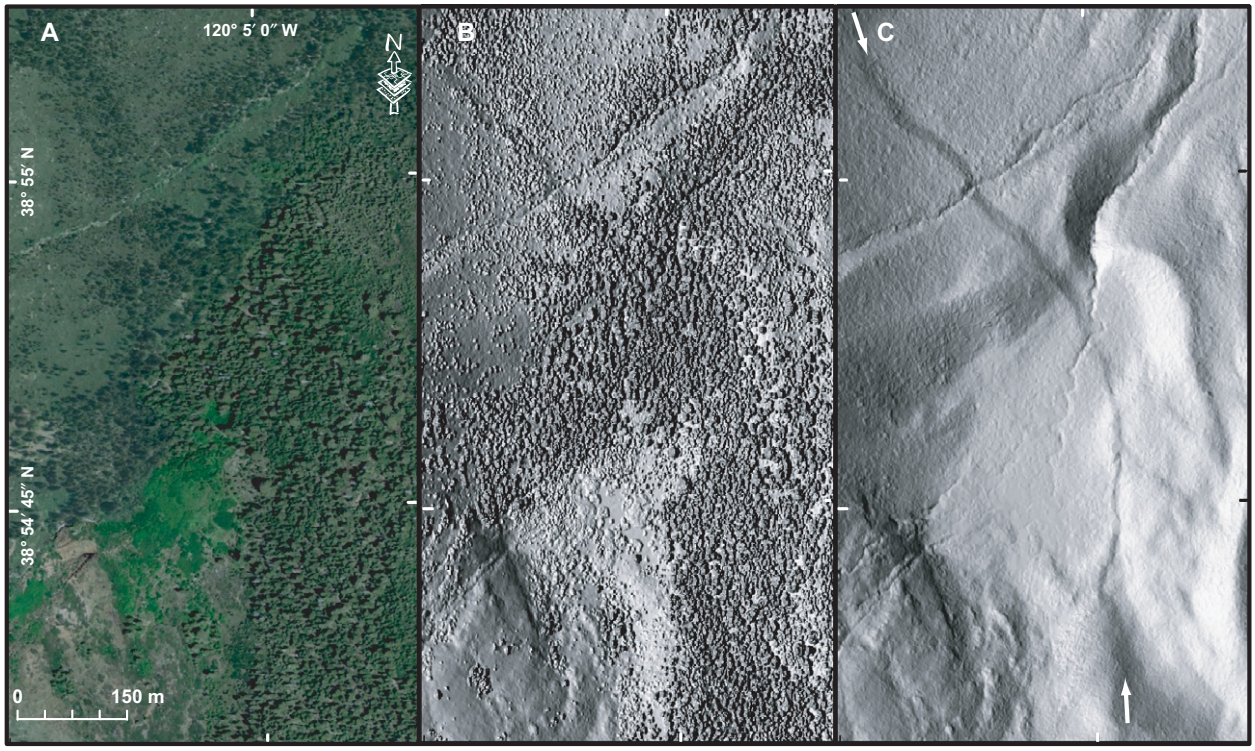

Figure 1. Comparison of color aerial photography with airborne light detection and ranging (LiDAR) imagery. (A) Color aerial orthophoto for part of range front along eastern base of Mt. Tallac with geomorphic features obscured by dense forest cover. See Figure 2 for location. (B) Same scene, first-return LiDAR imagery. (C) Same scene, last-return (bare-earth) LiDAR imagery showing range-front fault scarp (between white arrows) cutting colluvium, alluvium, and Tioga moraine. See Mt. Tallac segment for discussion.

tectonic features. These features include linear scarps in unconsolidated alluvium, colluvium, and glacial moraines; triangular facets in unconsolidated glacial till; linear side-slope troughs aligned with scarps in moraine crests; antithetic scarps; closed depressions; hanging-wall grabens; back-tilted moraine crests; and saddles in ridgelines.

Most of the localities and features described in this paper had previously been studied in the field prior to acquisition of the LiDAR data, and preliminary interpretations had been made (Schweickert et al., 2000, 2004; Howle, 2000). Despite difficult access in steep densely vegetated terrain, our detailed field mapping (1:12,000 scale) led to the recognition of numerous scarps cutting glacial moraines and tectonic geomorphic features such as those just listed. Dense forest cover in most areas meant that conventional aerial photography was of little use (Fig. 1).

Acquisition of the LiDAR data has enabled bare-earth visualization of key tectonic features and confirmation of most features originally mapped. The bare-earth LiDAR data have improved and clarified the original mapping and have led to identification of some features not originally recognized in the field, such as low-relief scarps on moraine side slopes and landslide deposits. Importantly, the high-resolution topography has been used for robust three-dimensional quantification of tectonic displacement across individual fault strands.

GEOCHRONOLOGY OF FAULTED DEPOSITS

In the central and southern Sierra Nevada, many detailed studies have presented age limits for the glacial chronology (Gillespie, 1984; Gillespie et al., 1984; Phillips et al., 1990, 1996, 2009; Bursik and Gillespie, 1993; Clark and Gillespie, 1997). In the northern Sierra Nevada, however, modern analytical age determinations are few. Correlations of glacial moraines based on relative weathering criteria are complicated by differences in precipitation, types of boulders, and the effects of wildfires on boulder spalling due to differences in fuel weights (Burke and Birkeland, 1979).

To estimate maximum and minimum limiting ages of glacial deposits displaced along faults in the study area, we established age limits for the Tahoe and Tioga glaciations using new ^{10}Be and ^{26}Al terrestrial cosmogenic nuclides (TCN) and optically stimulated luminescence (OSL) age dates. We then correlated these new data from the study area with other data from the Lake Tahoe region, geochronologic data from the southern Sierra Nevada, and the global marine isotope stages (MIS).

During the late Pleistocene, the Crystal Range, southwest of Lake Tahoe, was covered by a broad ice cap centered over Rockbound Valley. This ice cap extended east across the Sierran crest (McAllister, 1936; Wahrhaftig and Curtis, 1965) and fed outlet glaciers into the Tahoe Basin (Fig. 2). The outlet glaciers emerged from the deep canyons, crossed range-front faults of the Tahoe-Sierra frontal fault zone, and deposited prominent lateral and medial moraines that extend 2.5–7 km beyond the range front. Morainal deposits from the late Pleistocene Tahoe and Tioga glacial stages have been displaced by the Tahoe-Sierra frontal fault zone and provide a record of post-depositional strain, which, combined with the glacial chronology, define tectonic slip rates for the Tahoe-Sierra frontal fault zone. See GSA Data Repository for descriptions of the Tahoe- and Tioga-age glacial deposits and stratigraphy (see footnote 1).

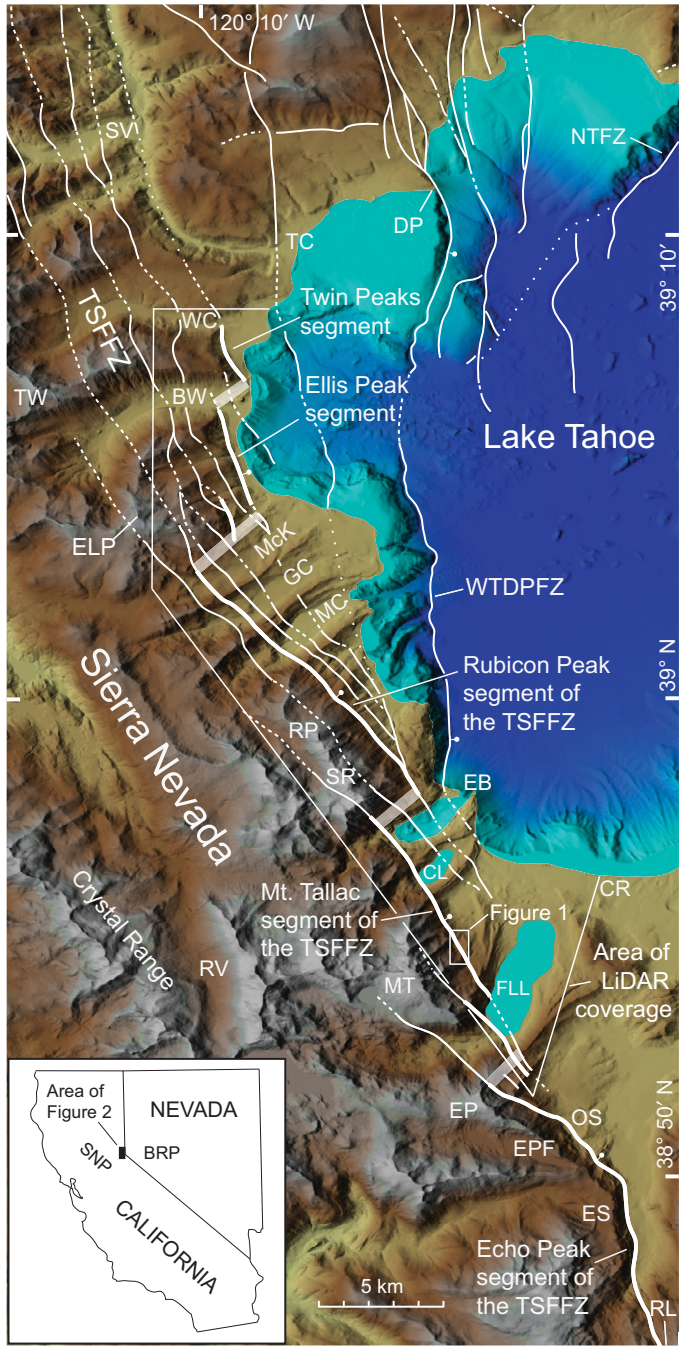

Figure 2. Shaded relief map of western part of the Lake Tahoe basin, California. Map shows area of airborne LiDAR coverage, mapped faults, and selected geographic locations discussed in text. Faults are dashed where approximately located, dotted where concealed, bar and ball on downthrown side. Heavier line weight shows principal range-front fault strands of the Tahoe-Sierra frontal fault zone (TSFFZ). Opaque white boxes indicate approximate segment boundaries and right steps in range front separating principal fault strands. Mapped faults are modified from Schweickert et al. (2000). BRP—Basin and Range Province; BW—Blackwood Creek; CL—Cascade Lake; CR—Camp Richardson; DP—Dollar Point; EB—Emerald Bay; ELP—Ellis Peak; EP—Echo Peak; EPF—Echo Peak fault; ES—Echo Summit; FLL—Fallen Leaf Lake; GC—General Creek; MC—Meeks Creek; McK—McKinney Creek; MT—Mt. Tallac; NTFZ—North Tahoe fault zone; OS—Osgood Swamp; RL—Round Lake; RP—Rubicon Peak; RV—Rockbound Valley; SNP—Sierra Nevada microplate; SR—Stony Ridge; SV—Squaw Valley; TC—Tahoe City, California; TW—Twin Peaks; WC—Ward Creek; WTDPFZ—West Tahoe–Dollar Point fault zone.

Limiting Ages of the Tioga Maximum Moraines

Our new TCN exposure age of 20.8 ± 1.4 ka for the largest and longest Tioga moraine (Tioga maximum) at Meeks Creek (see TCN discussion in GSA Data Repository and Data Repository Table DR1 [see footnote 1]) is consistent with radiocarbon age control at a site ~30 km southeast, where the Tioga maximum had previously been dated at ≥20.5 ± 0.6 ka (Clark et al., 2003). In the Bear River drainage, ~60 km northwest of Meeks Creek, the Tioga maximum occurred at 18.6 ± 1.2 ka (James et al., 2002). These data from the Lake Tahoe region indicate that the Tioga maximum advance occurred between ~ca. 19 and 21 ka, which correlates well with the Tioga 2 stage of Phillips et al., 2009 (see Table 1, this paper). In the central and southern Sierra Nevada, the Tioga maximum is correlated with the Tioga 1 stage between 25.2 ± 2.5 ka (Bursik and Gillespie, 1993) and 26.5 ± 1.7 ka (Phillips et al., 2009). In this study, we have considered the possibility that the highest Tioga moraines in other valleys between Fallen Leaf Lake and McKinney Creek, where we do not have site-specific chronology, may have been deposited during the older Tioga 1. Therefore, for calculation of tectonic slip rates along the Tahoe-Sierra frontal fault zone, we use the ≥20.5 ka age (Clark et al., 2003) as a minimum bound and the 26.5 ka age (Phillips et al., 2009) as a maximum bound and use the average value of 23.5 ± 3 ka as a broad and conservative estimate for the age of the Tioga maximum moraines.

TABLE 1. STRATIGRAPHIC RELATIONSHIPS OF SELECTED QUATERNARY MAP UNITS SHOWN IN FIGURES AND DISCUSSED IN TEXT, CORRELATION TO MARINE ISOTOPE STAGES (MIS), AND PUBLISHED AGE ESTIMATES

Glaciation and map unit	MIS stage and published age estimates (ka)
Tioga deglaciation	14.1 ± 1.5*
(Maximum limiting age of post-Tioga deposits; Qal)	14.5 ± 0.5†
Tioga glaciation	MIS 2 (13–32)§
(Qti)	
Tioga 2	Ca. 19–21#
	18.6 ± 1.2*
	≥20.5 ± 0.6**
Tioga 1	26.5 ± 1.7#
	<25.2 ± 2.5††
Tahoe glaciation	MIS 4 (64–75)§
(Qta)	
(Tahoe II)	65.8§§
	Ca. 70 ± 5##
	64.0 ± 3.5–76.4 ± 3.8*
Pre-Tahoe	≥MIS 6 (128–195)§
(pQta)	
(Donner Lake ?)	Ca. >131***
	Ca. 400 to 600†††

*James et al. (2002).
†Clark and Gillespie (1997).
§Shackleton and Opdyke (1976).
#Phillips et al. (2009).
**Clark et al. (2003).
††Bursik and Gillespie (1993).
§§Phillips et al. (1990), maximum age, $n = 6$.
##Gillespie (1991).
***Yount and LaPointe (1997).
†††Birkeland (1964).

Age Determinations for the Tioga Deglaciation

The Tioga deglaciation has been estimated at 14.5 ± 0.5 ka and 14.1 ± 1.5 ka in the central and northern Sierra Nevada, respectively (Clark and Gillespie, 1997; James et al., 2002; Table 1). Paleo–lake-level data from the terminus of the Truckee River (Lake Tahoe) drainage, which serves as a proxy for Tioga deglaciation, indicate that deglaciation occurred by 13.3 ± 0.3 ka (Benson et al., 1990). For this study, we have assumed that the Tioga deglaciation was concluded by 14.0 ± 1.0 ka.

Limiting Ages for the Tahoe Moraines

Our new analytical data for Tahoe moraines at Meeks Creek (TCN exposure age of 69.2 ± 4.8 ka; Table DR1 [see footnote 1]) correlate with the early Wisconsin (MIS 4) or younger Tahoe II glaciation (Gillespie, 1984). Our exposure age is corroborated by new optically stimulated luminescence (OSL) age data from Fallen Leaf Lake, where silty lacustrine sediment that underlies a Tahoe terminal moraine provides a maximum limiting age of 73.2 ± 8.7 ka for the Tahoe glaciation in the type locality (see OSL discussion in GSA Data Repository [see footnote 1]). In the Bear River drainage, TCN exposure ages of 64.0 ± 3.5 and 76.4 ± 3.8 ka have been reported for the highest and presumably oldest late Pleistocene till (James et al., 2002). These ages closely bracket the (64–75 ka) limiting bounds of MIS 4 (Shackleton and Opdyke, 1976; Table 1). On the basis of the coherence of these data with the MIS 4 boundaries, we use the 64–76 ka ages for the probable age range of the Tahoe moraines in the study area and use the average value of 70 ± 6 ka for calculating tectonic slip rates along the Tahoe-Sierra frontal fault zone.

TAHOE-SIERRA FRONTAL FAULT ZONE

The LiDAR imagery confirms that the Tahoe-Sierra frontal fault zone is the westernmost fault zone in the Lake Tahoe basin and forms the true neotectonic boundary between the Sierra Nevada microplate and the Basin and Range Province between 38°48′N and 39°18′N latitude (Schweickert et al., 2000, 2004). The prominent east-side-down range-front normal faults extend 45 km from Round Lake, 7 km south of Echo Summit, to Ward Canyon on the north, where less prominent faults continue northwest in bedrock (Fig. 2). At Fallen Leaf Lake, Emerald Bay, McKinney Creek, and Blackwood Creek, the range-front faults make en echelon right steps, where the eastern strands typically overlap for ~5 km or more with the western strands, and both sets of faults gradually lose displacement and topographic expression in the overlap areas. The segmented range-front fault zone includes five active fault segments, here named after the highest peaks in the corresponding footwall blocks. The segments from south to north are: Echo Peak, Mt. Tallac, Rubicon Peak, Ellis Peak, and Twin Peaks (Fig. 2). The segment boundaries are primarily defined by the right steps, which vary in width between 1 and 4 km and correspond with changes in the geomorphic character of the range-front fault and with changes in the trend of the range front. Across each step, the eastern strands strike slightly more northerly than the western strands, so that the zone broadens northward. Our analysis focuses on the Mt. Tallac and Rubicon Peak segments, where offsets in late Pleistocene glacial and Holocene alluvial deposits afford the best opportunity to characterize separation rates along the Tahoe-Sierra frontal fault zone.

Mt. Tallac Segment

The Mt. Tallac fault bounds the >1-km-high range front between Fallen Leaf Lake and Emerald Bay and extends 20 km from the south side of Fallen Leaf Lake through the headwaters of Meeks Creek west of Stony Ridge (Fig. 2; see GSA Data Repository Fig. DR1 for geologic map [see footnote 1]). The LiDAR imagery reveals a 5-km-long fault scarp from the southwest corner of Fallen Leaf Lake to the south shore of Cascade Lake (Figs. 3 and 4). On the north side of Cascade Lake, subtle scarps extend up the side slope to a 3-m-high scarp in the Tioga moraine crest (Figs. 4D and 4E). Northwest of this point, the fault is marked by offsets in undifferentiated colluvium and bedrock, and then it continues beneath historic rockslides at the head of Emerald Bay. On the north side of Emerald Bay, the Mt. Tallac fault has displaced a left-lateral moraine of Tioga age and then lies within a deep bedrock gully along the southwest buttress of Stony Ridge (Fig. 5B). From there, it controls the northwest-trending headwaters of Meeks Creek west of Stony Ridge (Fig. DR2 [see footnote 1]).

At Tallac Creek, 1.5 km northwest of Fallen Leaf Lake (Figs. 1 and 3; Fig. DR3 [see footnote 1]), we used the three-dimensional (3-D), point-cloud LiDAR data along with a new 3-D technique to measure the latest Pleistocene–Holocene vertical separation and extension on the Mt. Tallac fault. At this site, horizontal alluvium impounded by a Tioga-age terminal moraine (McCaughey, 2003) has been offset by the prominent Mt. Tallac range-front fault. Six topographic profiles across the offset post-Tioga alluvium were extracted from the LiDAR

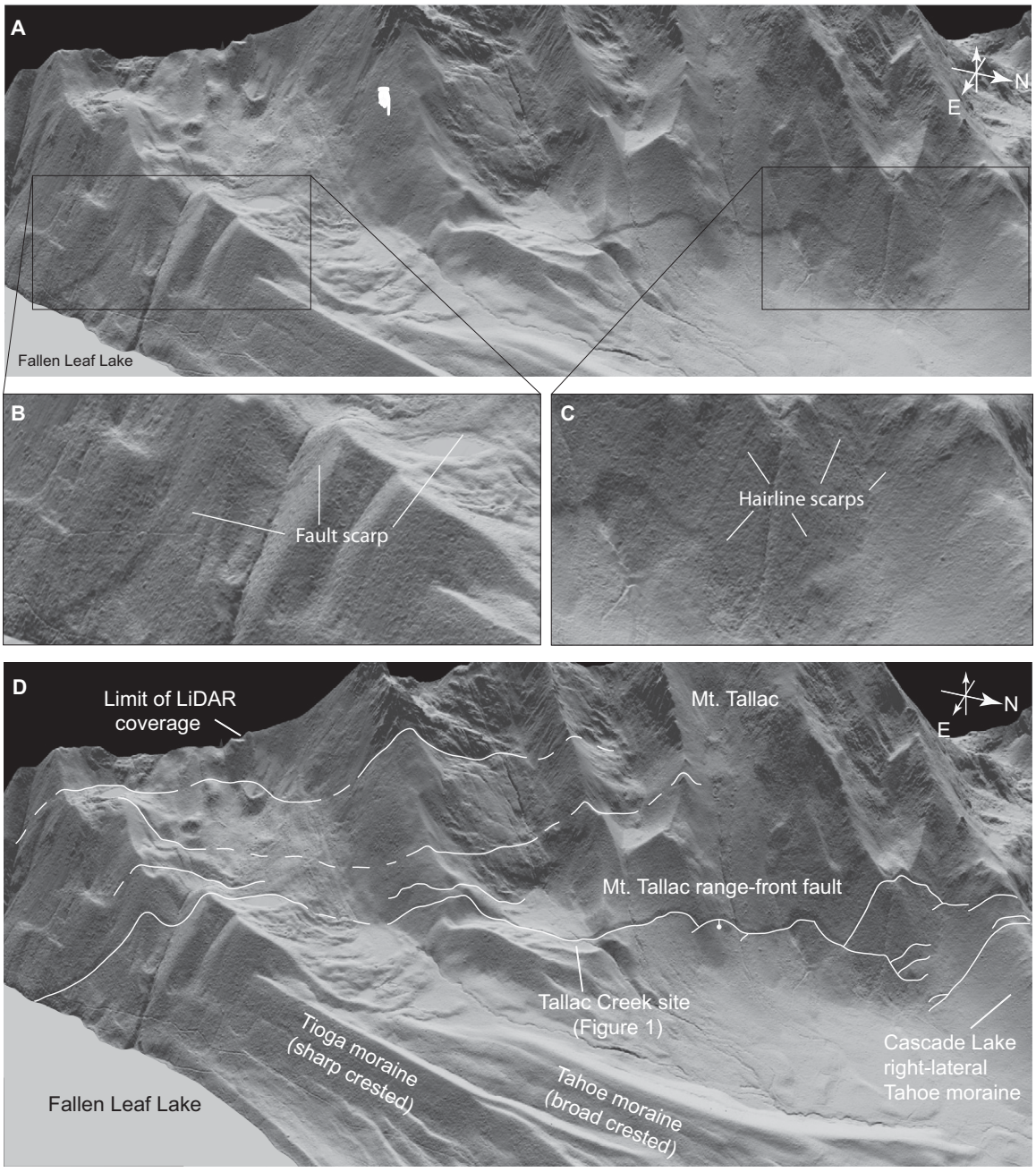

Figure 3. Oblique bare-earth LiDAR image of Mt. Tallac range-front fault. (A) View is to the west-southwest extending from Fallen Leaf Lake to the Cascade Lake right-lateral moraine, a horizontal distance of ~4.5 km along the base of the range front. Vertical exaggeration is 1.75. Hand icon shows illumination direction. (B) Detail of fault scarp above Fallen Leaf Lake. (C) Detail of diffuse ground-rupture traces and hairline scarps southeast of Cascade Lake. (D) Annotated view in A, showing the nearly continuous, 4.5-km-long range-front scarp of the Mt. Tallac fault, and selected geographic features. Faults are dashed where approximately located, bar and ball on downthrown side. Note the linear, evenly graded (unfaulted) Tioga and Tahoe moraines north of Fallen Leaf Lake. See Figure DR1 for geologic map of the Mt. Tallac range front (see text footnote 1).

data and modeled for vertical separation and extension (see Figs. DR3B and DR3C [see footnote 1]). We constructed these profiles, ranging from 69 to 159 m in length, by extracting a 2-m-wide swath of the LiDAR point cloud data and projecting the points into the vertical planes of the profiles (Fig. DR3 [see footnote 1]). This swath-sampling technique effectively integrates several closely spaced profiles from the point cloud into a single profile with greater data density. On the basis of 3-D modeling of fault planes in the study area (see Fig. DR4 [see footnote 1]), the Mohr-Coulomb failure criteria for normal faults (McCalpin, 1996), and field observations of dips of range-front faults in the Basin and Range Province (Slemmons, 1957; Bateman, 1965; Wallace, 1977; Clark et al., 1984), we modeled fault planes with dips

of 50°, 60°, and 70°. The modeled fault planes, which are perpendicular to the profiles, intersect the midpoint of the steepest slope segment in the scarp profile. If the extracted profile were linear between the scarp crest and toe, then modeled fault planes would intersect the midpoint of the linear segment (Bursik and Sieh, 1989). Then, we modeled LiDAR ground points in the hanging wall and footwall of the profile as best-fit vectors using a linear regression (Fig. DR3E [see footnote 1]). Intersections between the far-field vectors and modeled fault planes define piercing points from which the vertical separation and extension were extracted (Figs. DR3C and DR3F [see footnote 1]).

Analysis of the six profiles at Tallac Creek produced an average vertical separation of 3.8 ± 0.9 m and an extension of 2.2 ± 0.7 m, assuming the fault dips 60°. It is assumed that the age of the Tioga deglaciation (14.0 ± 1.0 ka) represents a maximum limiting age for the impounded alluvium and for the tectonic displacement; this age produces a minimum vertical separation rate of 0.3 ± 0.1 mm/yr and a minimum extension rate of 0.2 ± 0.05 mm/yr. Alternatively, if the impounded alluvium is significantly younger than the Tioga deglaciation, then Holocene separation rates may be higher.

A larger scarp in the Tioga moraine exists along strike, 150 m north of the displaced alluvium (Fig. DR3B [see footnote 1]). Model results from three topographic profiles across the scarp in the Tioga moraine indicate that an average 7.2 ± 0.9 m of vertical separation and 4.1 ± 0.5 m of extension have occurred since the Tioga moraine was deposited (23.5 ± 3 ka). These results give a vertical separation rate of 0.3 ± 0.1 mm/yr, i.e., the same rate as that determined in the adjacent alluvium, suggesting that a relatively constant strain rate has prevailed in the latest Pleistocene–Holocene.

Rubicon Peak Segment

At Emerald Bay, the Tahoe-Sierra frontal fault zone makes a 1.8-km-wide, en echelon right step to the northeast to the Rubicon Peak fault (Figs. 2, 4, and 5). This fault extends from ~2 km southeast of Cascade Lake toward the northwest at least as far as the head of Squaw Valley, a distance of 36 km (Fig. 2). Near the southeast end of the Rubicon Peak fault, late Pleistocene–Holocene displacement has been relatively small and has formed extensional fault-propagation folds in the Emerald-Cascade medial moraines (Fig. 5). However, 1.6 km along strike to the northwest, on the north side of Emerald Bay, displacement is greater, and the left-lateral Tioga and Tahoe moraines there are clearly displaced. New high-resolution digital bathymetry of Emerald Bay reveals scarps that displace post-Tioga landslide deposits on the bottom of the bay (Figs. 4 and 5). These scarps align with those in the left-lateral Tioga and Tahoe moraines (Fig. 5; Fig. DR2 [see footnote 1]). North of Emerald Bay, the Rubicon Peak fault forms the steep, linear, and 900-m-high, northwest-trending range front, where, along the oversteepened slope at the base of Stony Ridge, scarps are within colluvium and landslide deposits (Fig. 5; Fig. DR2 [see footnote 1]). Along strike northwest of Rubicon Peak, the fault crosses the heads of Meeks, General, and McKinney Creeks, where bedrock spurs are truncated and triangular facets are near the contacts with the morainal complexes (Fig. 6; Fig. DR5 [see footnote 1]). North of McKinney Creek, where the fault continues into the footwall of the Ellis Peak segment, displacement decreases abruptly. As far northwest as Squaw Valley, however, the Rubicon Peak fault forms steps and saddles in ridgelines and deep gullies in the side slopes of valleys.

Two kilometers north of Emerald Bay, the Rubicon Peak fault splays into several northwest-striking faults that are subparallel to and east of the range front (Fig. 2; Figs. DR2 and DR5 [see footnote 1]). Where these faults cut the glacial moraine complexes of Meeks, General, and McKinney Creeks, the bare-earth LiDAR imagery exposes a classic array of tectonic geomorphic features in tectonically disrupted lateral moraines. These features include side-slope troughs aligned with scarps in moraine crests, tectonically rotated (back-tilted) moraine crests, hanging-wall grabens, extensional fault-propagation folds, and tectonic reversal of the crests of Tioga and Tahoe moraines across the range-front faults (Figs. 6 and 7).

TECTONIC GEOMORPHOLOGY OF FAULTED LATERAL MORAINES

Classical scarp morphology of normal faults along range-front settings has long been recognized and documented throughout the Basin and Range Province (Gilbert, 1890; Slemmons, 1957; Witkind, 1964; Wallace, 1977; among others). The tectonic geomorphology of glacial moraines that have been disrupted by normal faults, however, has received far less attention. In this section, we describe distinctive tectonic landforms along the Tahoe-Sierra frontal fault zone. Some of these tectonic features, especially those east of the range front, are subtle and diffuse in nature, owing to their development in relatively thick unconsolidated deposits above an imbricate bedrock fault zone. Important geomorphic differences exist between range-front faults cutting colluvial/alluvial deposits and the tectonic features where normal faults cut lateral moraines. While most of these tectonic features in faulted glacial moraines have been documented elsewhere in the eastern Sierra Nevada, they have not been imaged as clearly as they are here.

Figure 4 (*on following page*). Oblique bare-earth LiDAR image of Cascade Lake and Emerald Bay, showing Mt. Tallac, Stony Ridge, and Rubicon Peak faults. (A) View to the west-southwest, showing fault-bounded range front from Cascade Lake right-lateral moraines to the south end of Stony Ridge, 1.8 km en echelon right step to Rubicon Peak fault, and high-resolution bathymetry of Emerald Bay (see GSA Data Repository regarding the new digital bathymetry [see text footnote 1]). Distance along bottom of image is 4.3 km. Hand icon shows illumination direction. Vertical exaggeration is 1.5 for all images. (B) Annotated view of A: MTF—Mt. Tallac fault zone; SRF—Stony Ridge fault; RPF—Rubicon Peak fault zone. (C) Scarp in Cascade Lake right-lateral Tioga moraine. (D) Tectonic geomorphology discussed in text. (E) View to the south-southeast showing tectonic features in D.

Fault Scarps in Lateral Moraines

Crests of unfaulted lateral moraines are generally linear and evenly graded with the crest sloping 2°–3° down canyon (note the smooth and linear crests of the unfaulted Tioga and Tahoe moraines in Fig. 3D). A primary indicator of fault disruption of a moraine crest is the abrupt termination and offset of the crest, with a scarp separating the two undisturbed segments (Figs. 7A and 7B; Fig. DR6 [see footnote 1]). Scarps are commonly best preserved along the moraine crests, compared to other landforms, because the coarse and poorly sorted deposits retain steep slopes for relatively long periods of time (Bursik and Sieh, 1989; Berry, 1997). Cobble- to sand-sized particles eroded from a scarp, crossing a moraine crest, typically do not collect at the base of the scarp but rather are shed onto the side slopes of the moraine, preserving the scarp form. Scarps typically are held up and armored by concentrations of boulders, exposed as the sandy matrix of the moraine is eroded and shed downslope. Thus, fault scarps in moraines commonly have more boulders than the rest of the crest.

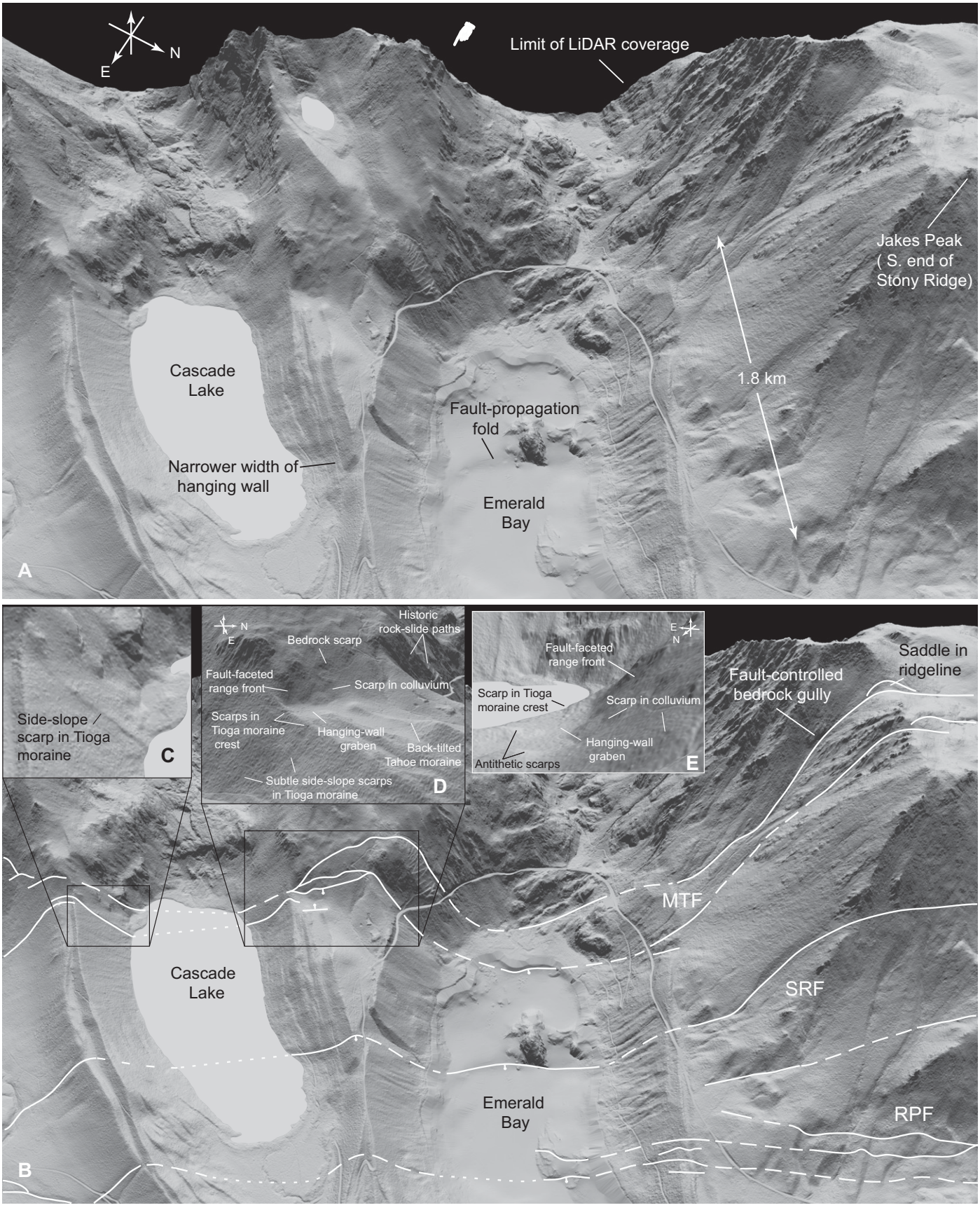
N
E
Limit of LiDAR coverage
Jakes Peak
(S. end of
Stony Ridge)
1.8 km
Cascade
Lake
Fault-propagation
fold
Narrower width of
hanging wall
Emerald
Bay
A
Side-slope /
scarp in Tioga
moraine
C
Historic
rock-slide paths
Bedrock scarp
Fault-faceted
range front
Scarp in colluvium
Scarps in
Tioga moraine
crest
Hanging-wall
graben
Back-tilted
Tahoe moraine
Subtle side-slope scarps
in Tioga moraine
D
Fault-faceted
range front
Scarp in Tioga
moraine crest
Scarp in colluvium
Hanging-wall
graben
Antithetic scarps
E
Saddle in
ridgeline
Fault-controlled
bedrock gully
MTF
SRF
RPF
Cascade
Lake
Emerald
Bay
B

Figure 4.

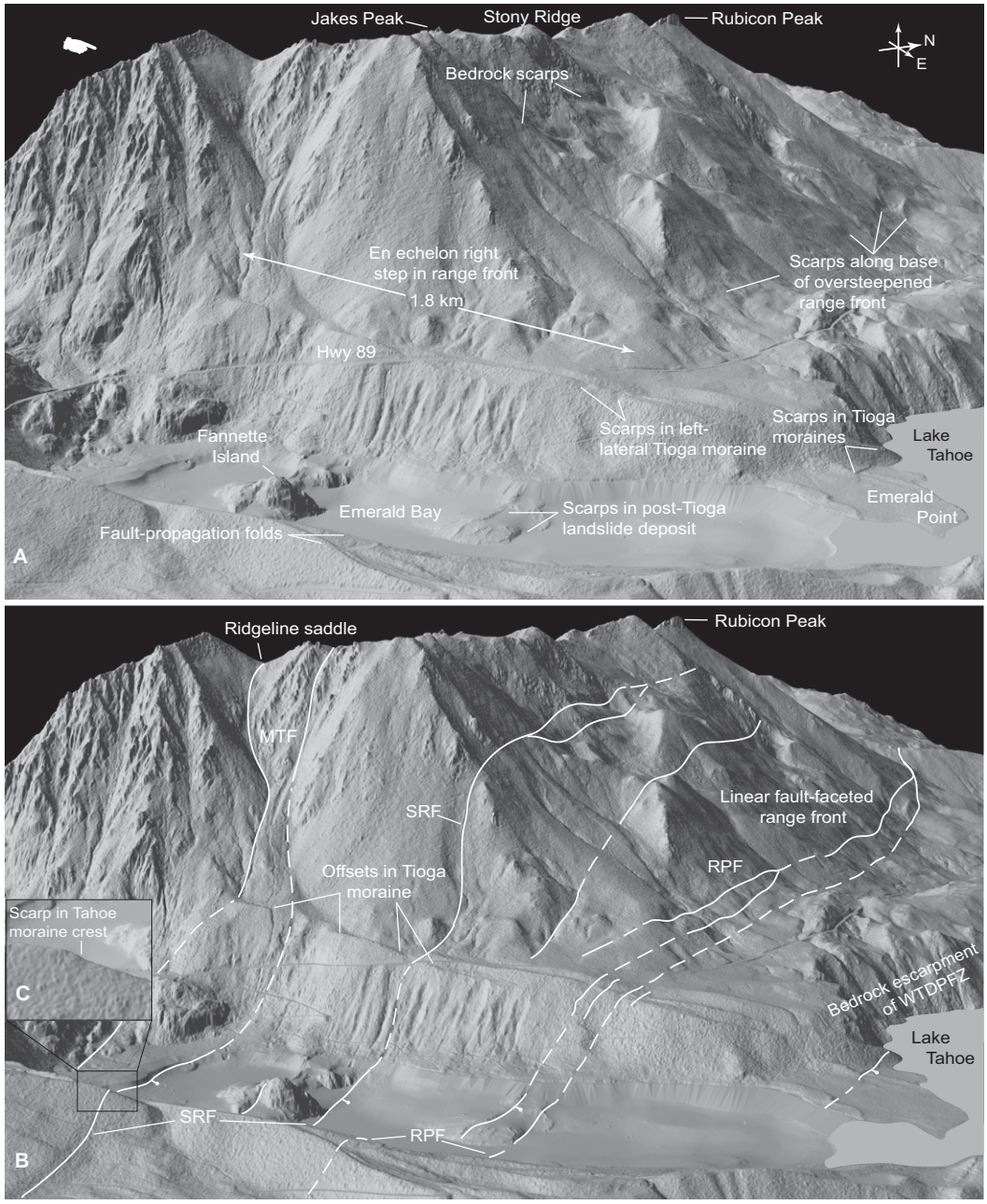

Figure 5. Oblique bare-earth LiDAR image of Stony Ridge and bathymetry of Emerald Bay. (A) View is to the west-northwest, showing en echelon right step in range front, linear fault-bounded range front north of Emerald Bay, tectonic geomorphology, and selected geographic features discussed in text. Hand icon shows illumination direction. Vertical exaggeration is 1.4. Distance across bottom of image is 2.4 km. (B) Faults discussed in text; dashed where approximately located, bar and ball on downthrown side. MTF—Mt. Tallac fault zone; RPF—Rubicon Peak fault zone; SRF—Stony Ridge fault; WTDPFZ—West Tahoe–Dollar Point fault zone. (C) Detail of scarp in Tahoe moraine.

Where fault displacement produces large, dip-slip separations (tens of meters), triangular facets typically separate the offset moraine crests (Fig. 7A). Oblique separation of moraine crests may form trapezoidal facets and offset side slopes (Fig. DR7A [see footnote 1]). Scarps in unconsolidated (cohesionless) moraines may display a "simple" scarp form at one location, whereas nearby along strike, there may be a complex, stepped scarp or a scarp with localized back-tilting (sag) and/or hanging-wall graben, similar to features in faulted alluvium/colluvium along range-front settings (Gilbert, 1890; Slemmons, 1957; Witkind, 1964; Wallace, 1977). Where the deformation is distributed or in younger moraines with smaller displacements, the moraine crest may be draped or warped (e.g., Wallace, 1977).

Extensional Fault-Propagation Folds in Moraines

Most fault segments in the Tahoe-Sierra frontal fault zone have displacement gradients, with displacement approaching zero near fault tips. Near the tips of fault strands and segments, where displacement is small, monoclinal or extensional fault-propagation folds are commonly seen in the unconsolidated glacial cover, above a blind bedrock fault at depth (Figs. 5A and 7E). The displacement gradient along a fault may produce a spectrum of structures, ranging from a gentle monoclinal warp, to a more pronounced step-like fold with footwall antiform and hanging-wall synform (Fig. 7E), to a fully breached monocline where the moraine crest is truncated and the footwall antiform and hanging-wall synform have been offset and are separated by a scarp (Fig. 7A; Fig. DR8A [see footnote 1];

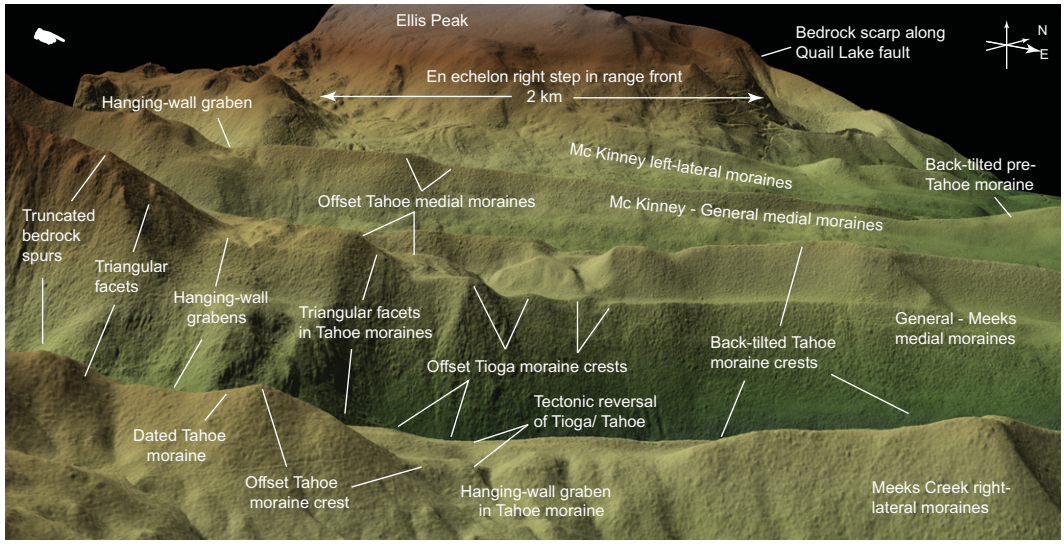

Figure 6. Tectonic geomorphology of faulted glacial moraines. Oblique bare-earth LiDAR image looking northwest across the faulted lateral and medial morainal complexes of Meeks Creek, General Creek, and McKinney Creek showing tectonic geomorphology discussed in text. Hand icon shows illumination direction. Vertical exaggeration is 1.75. Distance across the bottom of the image is 1.5 km. See Figure DR5 for geologic map (see text footnote 1).

Fraser et al., 1964; Hardy and McClay, 1999). Extensional fault-propagation folds are sometimes referred to as drape folds (e.g., Howard and John, 1997).

A fault-propagation fold may in some cases be distinguished from a moraine deposited across a preexisting scarp by the slopes and trends of the moraine crest segments on both sides of the inflection. The slopes of the crest segments on opposite sides of a fault-propagation fold are typically subparallel (except where the hanging wall has been back-tilted) and the crest segments are collinear (i.e., an initial linear feature deformed over a relatively short distance; Fig. 7E). In contrast, where a moraine was deposited over a preexisting topographic step (fault scarp), the moraine crest commonly veers inward toward the valley as the hanging wall is approached. This primary deflection of the moraine crest is a function of the discharge equation

$$Q = A \times V, \quad (1)$$

where A is the cross-sectional area of the glacier perpendicular to the flow path, V is the velocity of the glacier along the flow path, and Q is the ice-volume discharge. These relations and the conservation of ice mass over short distances require that, where a glacier flows down across a topographic step, the velocity increases, causing the cross-sectional area to decrease, and the glacier to constrict into the valley. In the case of a medial moraine separating two glaciers flowing down across a step, a single moraine is deposited on the footwall. Where the adjacent glaciers flow across the preexisting scarp (or step), the single medial moraine bifurcates into two lateral moraines with diverging crests. This depositional morphology occurs in the Tioga medial moraine between Cascade Lake and Emerald Bay (Fig. DR1 [see footnote 1]) and in the Tahoe medial moraine between Meeks and General Creeks (Fig. DR5 [see footnote 1]).

Additionally, a fault-propagation fold typically displays a smooth transition from footwall antiform to hanging-wall synform (Fig. 7E), whereas a moraine that was deposited during glacier flow over a preexisting scarp commonly has a sharp inflection point.

Side-Slope Troughs

In numerous places along the Tahoe-Sierra frontal fault zone, side-slope troughs are aligned with fault scarps in moraine crests (Fig. 7). These troughs are linear and are typically narrow and anomalously deep. Where the deformation was distributed across several fault strands, side-slope troughs may be broad swales. In some cases, troughs along the trace of a dipping fault conspicuously cut diagonally across the side slope (Fig. DR8A [see footnote 1]). Side-slope troughs are interpreted to have formed primarily from tectonic processes. Fault rupture at depth may produce a void in unconsolidated surficial deposits due to a listric fault geometry or fault-plane refraction (steepening) above the bedrock-till interface (Slemmons, 1957; Witkind, 1964; McCalpin, 1996). Coseismic opening of a void in unconsolidated surficial deposits sometimes causes rotational slumping of the hanging-wall deposits into the void and forms a depression along the strike of the fault (Gilbert, 1890; Slemmons, 1957; Witkind, 1964). Rotational slumping of unconsolidated hanging-wall deposits is analogous to Slemmons' (1957) "subsidence zone" and has also been referred to as "sag" (Fraser et al., 1964; Swan et al., 1980; Figs. DR6 and DR9F [see footnote 1]). Once a linear depression has been formed in the side slope of a moraine, slope processes such as dry ravel, sheetwash, grain flow, and debris flow operate along and within the side-slope trough, accentuating the feature.

Back-Tilted Moraine Crests

Throughout the Lake Tahoe basin, fault-bounded blocks are tilted westward toward east-dipping normal faults. At Fallen Leaf Lake and Cascade, Meeks, General, and McKinney Creeks, fault-bounded sections of colluvium and lateral moraines, which originally were deposited with an easterly gradient, are tectonically back-tilted toward the west or southwest (Figs. 4D, 6, and 7D; Fig. DR9A [see footnote 1]). Commonly, east-side-down scarps along faults bound the back-tilted sections. In some cases, long segments of moraine crests have zero gradient or 1°–2° slopes up-canyon. Tectonically back-tilted lateral moraines at or near the range front have been documented in at least six other locations in the eastern Sierra Nevada (Clark, 1967; Bursik and Sieh, 1989; Berry, 1997).

Lateral and medial morainal complexes typically have a triangular cross-sectional shape. Where the moraine complex has been tectonically back-tilted toward a normal fault, the topographically lower, up-valley part may be narrower than the topographically higher, down-valley part, which may be anomalously wide. This relationship is displayed by the back-tilted Tahoe-age moraines on both sides of Meeks Creek between faults D and E (Fig. DR5 [see footnote 1]).

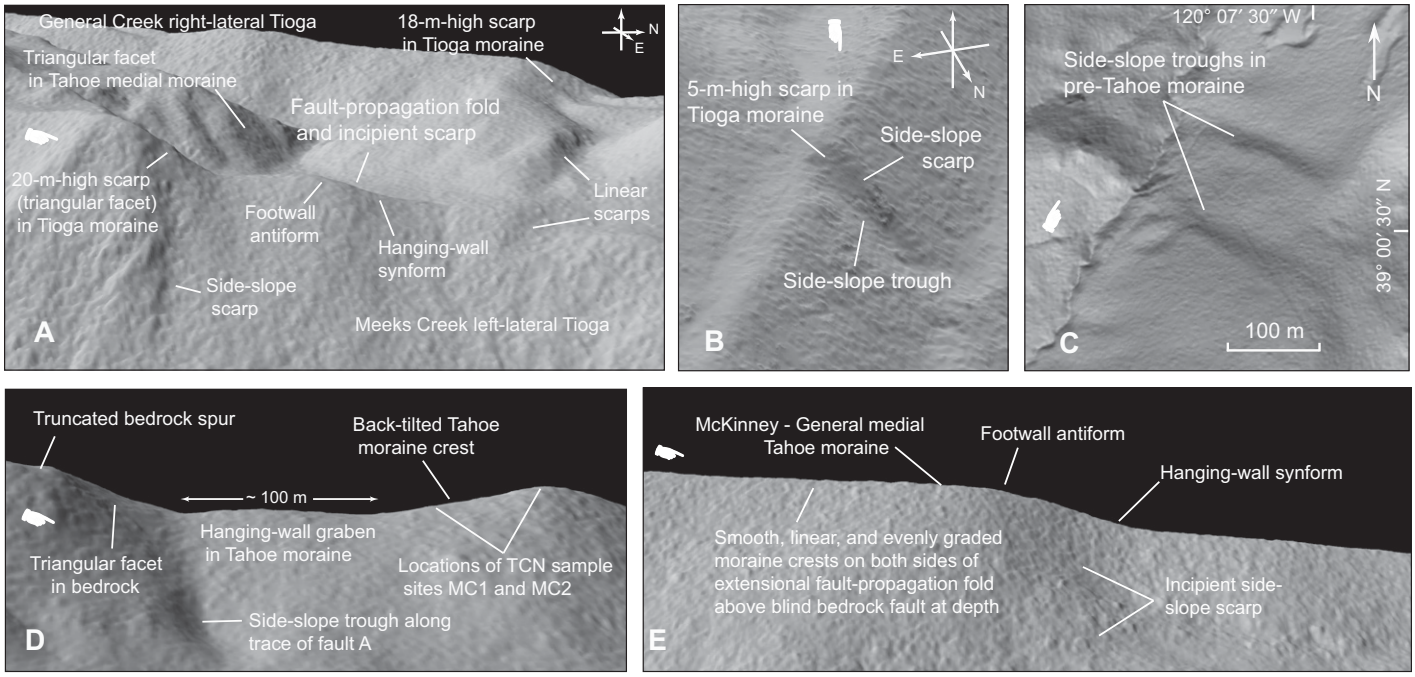

Figure 7. Examples of tectonic geomorphology along the Tahoe-Sierra frontal fault zone. See discussion regarding tectonic geomorphology of the Tahoe-Sierra frontal fault zone. Vertical exaggeration is 1.5 in all images unless otherwise noted. Hand icons show illumination direction. See Figure DR5 for geologic map and locations of insets (see text footnote 1). (A) Oblique view of medial moraine complex at Meeks and General Creeks highlighting various fault scarp morphologies discussed in text. View is to the west-northwest. Horizontal distance along Meeks Creek left-lateral Tioga moraine is ~450 m. (B) Oblique view of fault scarp and side-slope trough in Meeks Creek right-lateral Tioga moraine at fault E. View is to the south-southwest. Distance along offset Tioga moraine crest is ~200 m. (C) Plan view of NW-trending side-slope troughs in pre-Tahoe moraine on the south side of Lonely Gulch. (D) Horizontal perspective looking northwest at Meeks Creek right-lateral Tahoe moraine where it abuts bedrock, showing range-front tectonic features discussed in text and location of terrestrial cosmogenic nuclide (TCN) sampling sites. Vertical exaggeration is 1.25. (E) Horizontal perspective looking northwest at medial Tahoe moraine of McKinney Creek–General Creek, showing extensional fault-propagation fold. Width of image is ~700 m.

The absence of pre-Tahoe moraines along the range front, and their exposure at downvalley locations are also attributed to tectonic back-tilting (Fig. 6; Fig. DR5 [see footnote 1]). This relationship, where older, more extensive moraines have been tectonically down-dropped at the range front and subsequently buried beneath younger, less extensive moraines, has also been documented at seven other locations in the Sierra Nevada (Clark, 1967, 1972, 1979; Bursik and Sieh, 1989; Kelson et al., 1995; Berry, 1997). We consider this relationship to be compelling evidence of large displacements along the Tahoe-Sierra frontal fault zone during the Pleistocene.

Hanging-Wall Graben

Hanging-wall grabens are common along the Tahoe-Sierra frontal fault zone and vary in width from 30 to over 350 m (Figs. 4D, 4E, 6, and 7D; Figs. DR9A, DR10B, and DR11A [see footnote 1]). Most of the hanging-wall grabens along the Tahoe-Sierra frontal fault zone are closely associated (spatially and kinematically) with back-tilted moraines. As noted already, displacement on a curviplanar normal fault produces a near-surface void beneath the unconsolidated hanging wall. In some cases, a wedge-shaped section of the hanging wall collapses back into the void along antithetic or conjugate normal faults and produces a hanging-wall graben. Rotational displacement of a hanging-wall wedge on antithetic faults may decrease the amount of back-tilting (Swan et al., 1980). Consequently, hanging-wall grabens in lateral moraines may be expressed as sections of moraine crest with less back-tilt than is observed to the east of an antithetic structure (Fig. DR9A [see footnote 1]). Hanging-wall grabens also are expressed as broad low saddles with level moraine crests (Figs. 6 and 7D; Fig. DR9A [see footnote 1]). Hanging-wall grabens in lateral moraines at or near range-front faults have been documented in at least five other locations in the eastern Sierra Nevada (Clark, 1967; Bursik and Sieh, 1989; Berry, 1997); these are analogous to Slemmons' (1957) "gravity grabens."

Tectonic Reversal of Primary Depositional Position across a Range-Front Fault

Anomalous relationships exist between the heights of the Tioga- and Tahoe-age moraines on both sides of the range-front fault at Cascade Lake and Meeks and General Creeks. At these locations, in the footwall of the range front, the Tahoe moraines stand higher than the younger Tioga moraines, reflecting the primary depositional position of the moraines due to the greater thickness of the Tahoe glaciers compared to the Tioga glaciers (Birkeland, 1964; Clark, 1967). In the hanging wall across the range-front fault, however, the primary depositional position is reversed, and Tioga crests are topographically higher than Tahoe crests (Fig. 6; Figs. DR9A and DR9C [see footnote 1]). This reversal of the primary depositional position of the crests is attributed to two processes: tectonic displacement during the Tahoe-Tioga interglacial period that down-dropped the Tahoe moraine in the hanging wall, and aggradation in the hanging-wall valley. During the advance of the Tioga maxi-

mum glacier, the Tioga moraine crest on the hanging wall was deposited over, and partially buried, the down-dropped Tahoe moraine. The sum of the differences in elevation between the Tahoe and Tioga crests on both sides of the fault approximates the tectonic displacement (vertical separation) during the interglacial period (Clark, 1972; Berry, 1997). Tectonic range-front reversals of moraine crests have been documented in at least six other eastern Sierra Nevada locations (Clark, 1972, 1979; Bursik and Sieh, 1989; Berry, 1997).

Narrower Width of Moraine Complexes in the Hanging Wall

Down valley from the range front, where normal faults displace morainal complexes, dip-slip displacement causes the moraine complex to be narrower in the hanging wall than in the footwall over relatively short distances. In plan view, this is similar in appearance to an anticline cut by a transverse normal fault. In this case, topographic contours on the footwall block step inward along the fault and then continue along the hanging wall. This morphology is well exposed in the medial moraine complexes between Cascade Lake and Emerald Bay along the Stony Ridge fault (Fig. 4A) and in the Meeks Creek right-lateral moraine complex at fault F (Fig. DR5 [see footnote 1]).

NEW METHODS FOR MODELING TECTONIC DISPLACEMENTS OF FAULTED LATERAL MORAINES

The late Pleistocene moraines straddling the Tahoe-Sierra frontal fault zone are ideal geomorphic strain markers because the lateral moraines were originally linear and had continuous, evenly graded crests (note the smooth and linear crests of the unfaulted Tioga and Tahoe moraines in Fig. 3D). To model the tectonic displacement of moraine crests, we developed a new, three-dimensional (3-D), moraine-crest-reconstruction technique that utilizes the linear, far-field trend and the triangular cross-section geometry of lateral moraines. From the high-resolution 3-D LiDAR data, we reconstructed moraine crests on both sides of faults and used these crests as piercing lines (see Fig. DR7 [see footnote 1]).

A juvenile lateral moraine has a very sharp, linear crest and steep side slopes. As finer-grained till is gradually eroded from the crest and shed down the side slopes, the moraine crest is broadened, and the side slopes become less steep (Zreda et al., 1994; Putkonen and Swanson, 2003; see supplementary Glacial Deposits and Stratigraphy section [see footnote 1]). It is reasonable to assume, as in previous studies, that rates of moraine crest erosion and reduction of the side-slope angle are equal on both sides of a fault. This assumption is reasonable because the slope aspects on opposite sides of a moraine crest are the same on both sides of a fault and also because long-term precipitation is unlikely to vary significantly over the nominal distance that the footwall and hanging-wall sections are modeled. This assumption means that moraine crests on both sides of a fault will be lowered at the same rate over time, but the vertical separation between the moraine crests across fault scarps should only vary as a function of tectonic displacement.

In the moraine-crest-reconstruction method, piercing-line vectors are mathematically defined by the intersection of best-fit planes to the side slopes of the moraines (Fig. DR7 and see supplementary Mathematical Modeling of Planes and Vectors section [see footnote 1]). The piercing-line vectors are projected to intersect with fault planes dipping 50°, 60°, and 70°, defining coupled pairs of piercing points for each modeled fault plane. From these statistically significant piercing points, we extract the vertical separation and extension (Fig. DR7J [see footnote 1]).

In cases where the footwall or hanging-wall moraine lacks planar side slopes and the technique just described cannot be used, we employed an alternative technique, in which a piercing-line vector is fit to LiDAR ground points along the moraine crest with a linear regression. We refer to this method as a vector-fit model. See supplementary Mathematical Modeling of Planes and Vectors for a comparison of the moraine-crest-reconstruction and vector-fit techniques (see footnote 1).

In cases where the footwall and/or hanging wall have been rotated or where a piercing-line vector cannot be extracted from the landform, neither technique may be used. A less rigorous approach is to use the elevation difference between horizontal projections of footwall and hanging-wall strain markers to define the net tectonic vertical separation (e.g., Swan et al., 1980). This approach is independent of fault dip and provides only a rough estimate of the vertical separation.

Wherever possible, we employed both the moraine-crest-reconstruction and vector-fit techniques to determine a range of possible displacements. These values were then propagated into the error estimates of separation rates. The epistemic error estimates in separation rates reported in this study reflect (1) the range of displacement solutions determined by different modeling techniques, whenever possible, (2) a 20° range of assumed fault dips, and (3) a broad and conservatively estimated range of limiting ages that are not skewed toward a minimum. See GSA Data Repository for the calculation of root-mean-square error estimates (1 standard deviation) reported as ±1 standard deviation in this study (see footnote 1).

SUMMARY OF TECTONIC DISPLACEMENTS AND RATES ALONG THE RUBICON PEAK SEGMENT

On the basis of the geomorphic criteria and limiting ages described herein, and using our new techniques for modeling the cumulative tectonic displacement of lateral moraines, we determined the vertical separation rate and the extension rate at 15 locations along the Rubicon Peak segment (see supplementary Modeled Tectonic Displacements section for details of individual offsets [see footnote 1]). At three locations along the Rubicon Peak segment, we summed the model results across the width of the zone, yielding aggregate vertical separation and extension rates that provide a first-order approximation of the seismic moment (Fig. 8; see Table DR3 for summaries [see footnote 1]).

The maximum late Pleistocene–Holocene vertical separation rate along the Rubicon Peak segment was determined at the Meeks Creek–General Creek medial moraine complex. There, the offset Tioga moraines on both sides of the complex define an average aggregate vertical separation rate of 1.5 ± 0.4 mm/yr and an extension rate of 0.8 ± 0.2 mm/yr since 23.5 ± 3.0 ka. The rates decrease along strike to the northwest and southeast (Fig. 8). The Tahoe-age strain markers in the General Creek–McKinney Creek medial moraine to the north and the Meeks Creek right-lateral moraine to the south both yield aggregate vertical separation rates of 0.9 ± 0.3 mm/yr and extension rates of 0.5 ± 0.2 mm/yr since 70.0 ± 6.0 ka.

At Emerald Bay, fault displacement of the left-lateral Tioga moraine along the Rubicon Peak fault defines a vertical separation rate of 0.6 ± 0.1 mm/yr and an extension rate of 0.4 ± 0.1 mm/yr since 23.5 ± 3.0 ka.

The vertical separation and extension rates presented herein are considered minimum estimates because (1) the limiting ages represent a broad and conservatively estimated range that is not biased toward a minimum, (2) mapped faults in bedrock, across which we have no strain markers, are not included in the estimates, and (3) some faults that displace the glacial deposits cannot be evaluated with the airborne LiDAR imagery due either to resolution of the data or to complex morphology that precludes displacement analysis.

Figure 8 (*on following page*). Summary of vertical separation rates and extension rates along Tahoe-Sierra frontal fault zone. Vertical separation rates (VSR) and extension rates (EXR) discussed in text for major fault strands of the Mt. Tallac and Rubicon Peak segments of the Tahoe-Sierra frontal fault zone (TSFFZ), plotted on U.S. Geological Survey 10 m digital elevation model. Colored fault segments indicate the age of the faulted deposit, and line weights indicate the relative magnitude of the slip rate (see inset legend). Refer to GSA Data Repository Table 3 and Data Repository text for details of individual offsets (see text footnote 1). CL—Cascade Lake; EB—Emerald Bay; EP—Echo Peak; EPF—Echo Peak fault; FLL—Fallen Leaf Lake; HWF—Homewood fault; MT—Mt. Tallac; MTF—Mt. Tallac fault; QLF—Quail Lake fault; RP—Rubicon Peak; RPF—Rubicon Peak fault.

POTENTIAL EARTHQUAKE MAGNITUDES ALONG THE TAHOE-SIERRA FRONTAL FAULT ZONE

Using published relationships between subsurface-rupture area and observed earthquake magnitudes (Wells and Coppersmith, 1994), we estimated a range of potential earthquake moment magnitudes (M_w) that could be generated by future earthquakes along the Tahoe-Sierra frontal fault zone. Variables incorporated into these rupture scenarios include estimated surface-rupture lengths of 0.7, 0.8, 0.9, and 1.0 times our total mapped fault lengths and depths to the base of the seismogenic zone ranging from 10 km (Hawkins et al., 1986) to 18 km (Smith et al., 2004).

The range-front sections of the Echo Peak and Mt. Tallac faults may have ruptured coseismically in the latest Pleistocene–Holocene time frame, based on 3 m of vertical separation in the Tioga moraine at Osgood Swamp (McCaughey, 2003; Fig. 2), 3.8 ± 0.8 m vertical separation south of Fallen Leaf Lake (Fig. DR12 [see footnote 1]), 3.8 ± 0.9 m vertical separation at the Tallac Creek site (Fig. DR3 [see footnote 1]), and the youthful appearance of the fault scarps at all of these sites. The combined length of the range-front sections of the Echo Peak and Mt. Tallac faults is ~27 km (Fig. 2), which yields a range of potential earthquake magnitudes from 6.5 ± 0.25 to 6.7 ± 0.25. If only the Mt. Tallac fault (with a length of 20 km) were to rupture, earthquake magnitudes could range from 6.3 ± 0.25 to 6.6 ± 0.25 (see Table DR4 [see footnote 1]).

As previously noted, the southern half of the Rubicon Peak segment displaces late Quaternary deposits from southeast of Cascade Lake to the north side of McKinney Creek, a distance of 18 km. North of McKinney Creek, the Rubicon Peak fault projects into the bedrock footwall of the Ellis Peak segment and continues to at least Squaw Valley, another 18 km northwest. Two scenarios for the Rubicon Peak segment are considered herein: rupture of the southern half alone and rupture of the entire mapped length. The first scenario, which considers only that part of the range-front Rubicon Peak fault (fault A; Figs. DR2 and DR5 [see footnote 1]) with evidence of late Quaternary displacement (length of 18 km), yields earthquake magnitudes from 6.3 ± 0.25 to 6.6 ± 0.25 (Table DR5 [see footnote 1]). This part of the Rubicon Peak segment includes the fault splays parallel to the range-front fault (faults B, C, D, and E in Fig. DR5 [see footnote 1]) that we interpret as the complex surface rupture of two or more bedrock faults beneath the unconsolidated piedmont cover. The second scenario, which assumes that the entire mapped length of the Rubicon Peak fault ruptures (length of 36 km; Fig. 2), produces earthquake magnitudes between 6.6 ± 0.25 and 6.9 ± 0.25 (Table DR5 [see footnote 1]).

Comparison of the relatively fresh appearance of post-Tioga side-slope scarps along the Mt. Tallac segment (Fig. 4C) to the degraded and subdued appearance of post-Tioga side-slope scarps along the Rubicon Peak segment (Fig. DR9E [see footnote 1]) suggests that the two segments probably did not rupture coseismically during the last ground-rupturing earthquake along the Mt. Tallac segment. A future coseismic rupture scenario cannot be ruled out, however, because the en echelon right step is <2 km in width (Harris and Day, 1999; Wesnousky, 2006). This scenario has the longest rupture length considered herein but may not be a maximum because we do not include the West Tahoe–Dollar Point fault zone (Fig. 2). The total rupture length of the combined Mt. Tallac and Rubicon Peak faults is 42 km. This surface-rupture length produces a range of earthquake magnitudes from 6.5 ± 0.25 to 6.9 ± 0.25 (Table DR6 [see footnote 1]).

POSSIBLE EARTHQUAKE-TRIGGERED LANDSLIDES ALONG THE TAHOE-SIERRA FRONTAL FAULT ZONE RANGE FRONT

Rotational landslides and translational rockslides in close proximity to the mapped Mt. Tallac fault occur along the Mt. Tallac range front at the heads of Fallen Leaf Lake, Cascade Lake, and Emerald Bay (Fig. DR1 [see footnote 1]). Similarly, from Emerald Bay northwest along the oversteepened slope at the base of the Rubicon Peak range front, numerous landslides straddle and/or lie adjacent to the mapped range-front fault (Figs. DR2 and DR5 [see footnote 1]). In several places, fault scarps coincide with landslide head scarps, and in other places, the landslide deposits have been displaced by the Rubicon Peak fault. The close proximity of these mass-wasting features with mapped faults strongly suggests that they have been triggered by strong ground motion during earthquakes along the Tahoe-Sierra frontal fault zone.

CONCLUSIONS

The bare-earth LiDAR topography reveals a broad array of tectonic geomorphic features along the Tahoe-Sierra frontal fault zone west of Lake Tahoe, demonstrating late Pleistocene to Holocene activity along the fault zone and validating earlier mapping of the fault zone (Schweickert et al., 2000, 2004). This study utilized bare-earth LiDAR data, together with field data to identify, visualize, and characterize faults in a mountainous and heavily forested region. The tectonic geomorphic features of faulted lateral moraines described herein and illustrated with the bare-earth LiDAR imagery provide clearly defined examples for studies of range-front lateral moraines displaced and disrupted by normal faults elsewhere. The examples highlight the unique geomorphic features that develop in relatively thick unconsolidated lateral moraines above an imbricate bedrock fault zone away from the range front. This study also presents new three-dimensional methods utilizing the bare-earth LiDAR point cloud data for modeling tectonic displacements of range-front alluvium, colluvium, and glacial moraine crests. These methods have yielded statistically robust estimates of vertical separation and extension across fault arrays at 17 locations.

New terrestrial cosmogenic nuclide and optically stimulated luminescence age data from the study area have been combined with regional age data to establish limiting ages for the Tioga (23.5 ± 3 ka) and Tahoe (70 ± 6 ka) glaciations in the Lake Tahoe region, which correlate with marine isotope stages MIS 2 and MIS 4, respectively.

We coupled these numerically robust displacement models with the new age estimates to define vertical separation and extension rates at numerous localities for the past ~70 k.y. This data set on vertical separations and extensions

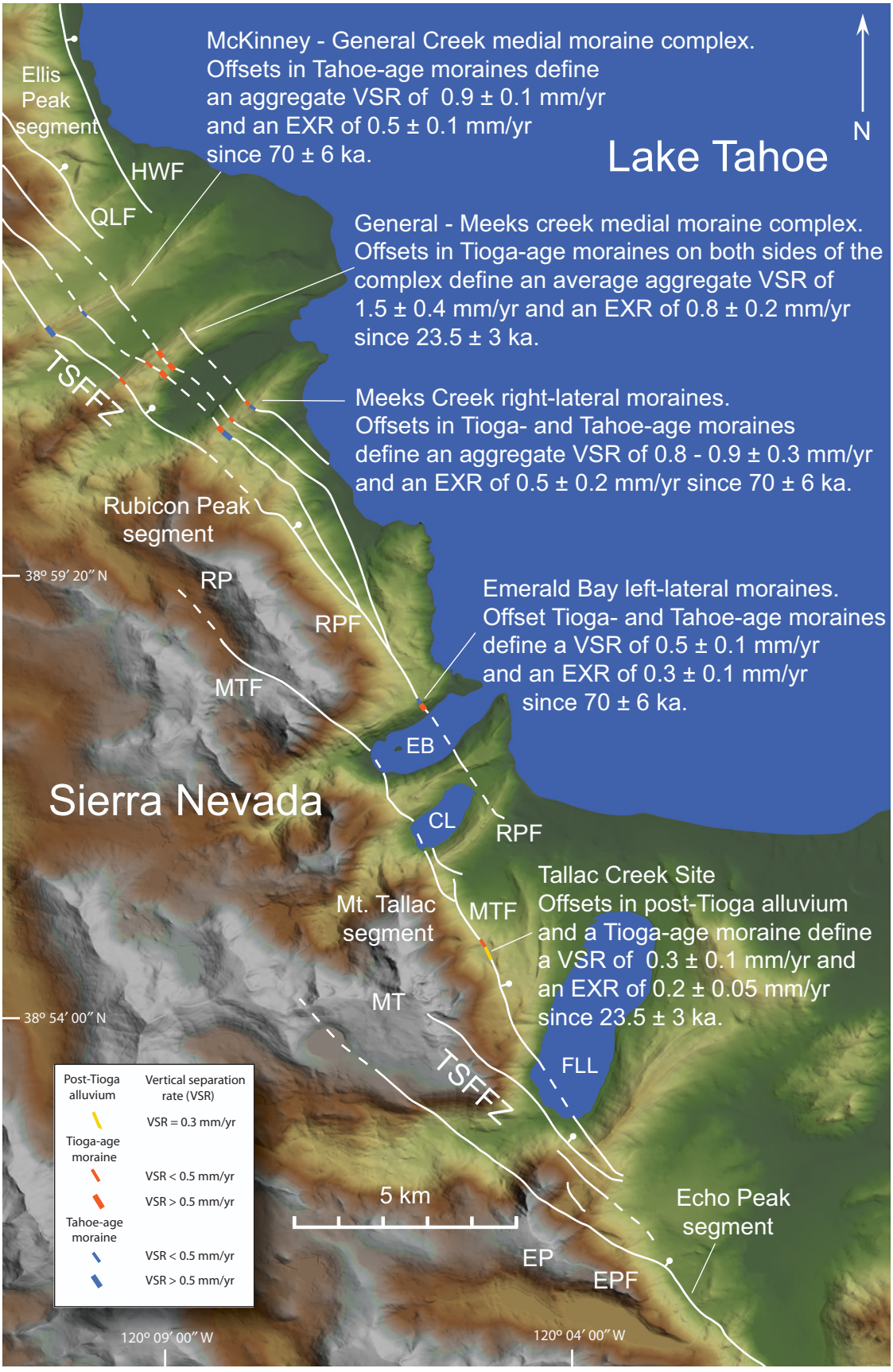
McKinney - General Creek medial moraine complex.
Offsets in Tahoe-age moraines define
an aggregate VSR of 0.9 ± 0.1 mm/yr
and an EXR of 0.5 ± 0.1 mm/yr
since 70 ± 6 ka.
Lake Tahoe
N
Ellis
Peak
segment
HWF
QLF
General - Meeks creek medial moraine complex.
Offsets in Tioga-age moraines on both sides of the
complex define an average aggregate VSR of
1.5 ± 0.4 mm/yr and an EXR of 0.8 ± 0.2 mm/yr
since 23.5 ± 3 ka.
TSFFZ
Meeks Creek right-lateral moraines.
Offsets in Tioga- and Tahoe-age moraines
define an aggregate VSR of 0.8 - 0.9 ± 0.3 mm/yr
and an EXR of 0.5 ± 0.2 mm/yr since 70 ± 6 ka.
Rubicon Peak
segment
38º 59′ 20″ N
RP
RPF
MTF
Emerald Bay left-lateral moraines.
Offset Tioga- and Tahoe-age moraines
define a VSR of 0.5 ± 0.1 mm/yr
and an EXR of 0.3 ± 0.1 mm/yr
since 70 ± 6 ka.
EB
Sierra Nevada
CL
RPF
Tallac Creek Site
Offsets in post-Tioga alluvium
and a Tioga-age moraine define
a VSR of 0.3 ± 0.1 mm/yr and
an EXR of 0.2 ± 0.05 mm/yr
since 23.5 ± 3 ka.
Mt. Tallac
segment
MTF
MT
38º 54′ 00″ N
FLL
TSFFZ
Post-Tioga alluvium
Vertical separation rate (VSR)
VSR = 0.3 mm/yr
Tioga-age moraine
VSR < 0.5 mm/yr
VSR > 0.5 mm/yr
Tahoe-age moraine
VSR < 0.5 mm/yr
VSR > 0.5 mm/yr
5 km
Echo Peak
segment
EP
EPF
120º 09′ 00″ W
120º 04′ 00″ W

Figure 8.

is much larger than that of any previous study in the region and allows a more complete characterization of the displacement and slip-rate histories of entire fault segments. The right-stepping, en echelon range-front segments of the Tahoe-Sierra frontal fault zone have progressively greater slip rates along strike to the northwest, an observation that is consistent with greater extension and structural relief in the northern part of the Lake Tahoe basin. The minimum vertical separation rate of 1.5 ± 0.4 mm/yr, along the Rubicon Peak segment, calculated herein, is two to three times greater than previously published "basinwide" estimates of vertical separation rates, which disregarded the Tahoe-Sierra frontal fault zone (Kent et al., 2005; Dingler et al., 2009). This study has also yielded a two- to threefold increase in the estimate of potential seismic moment in the Lake Tahoe basin, which highlights the importance of the Tahoe-Sierra frontal fault zone. This fault zone, which is potentially capable of generating moment magnitude 6.3 ± 0.25 to 6.9 ± 0.25 earthquakes, represents a substantial seismic hazard to the region. Numerous landslides and rockslides near mapped faults likely were triggered by earthquakes, implying that an associated coseismic mass-wasting hazard exists along the steep Tahoe-Sierra frontal fault zone range front.

ACKNOWLEDGMENTS

This study was funded, in part, by the U.S. Army Corp of Engineers, Dam Safety Assurance Program. JFH would like to thank Keith Kelson for his input during preparation of an early version of this paper. We are grateful for constructive colleague reviews by James Lienkaemper, Kenneth Hudnut, Andrew Cyr, and peer reviews by Arthur Sylvester and an anonymous reviewer, all of which improved the manuscript. Any use of trade, product, or firm names is for descriptive purposes only and does not imply endorsement by the U.S. government.

REFERENCES CITED

Arrowsmith, J.R., and Zielke, O., 2009, Tectonic geomorphology of the San Andreas fault zone from high resolution topography: An example from the Cholame segment: Geomorphology, v. 113, p. 70–81, doi:101016/j.geomorph. 2009.01.002.

Bateman, P.C., 1965, Geology and Tungsten Mineralization of the Bishop District, California: U.S. Geological Survey Professional Paper 470, 208 p.

Benson, L.V., Currey, D.R., Dorn, R.I., Lajoie, K.R., Oviatt, C.G., Robinson, S.W., Smith, G.I., and Stine, S., 1990, Chronology of expansion and contraction of four Great Basin lake systems during the past 35,000 years: Palaeogeography, Palaeoclimatology, Palaeoecology, v. 78, p. 241–286, doi:10.1016/0031-0182(90)90217-U.

Berry, M.E., 1997, Geomorphic analysis of late Quaternary faulting on the Hilton Creek, Round Valley and Coyote Warp faults, east-central Sierra Nevada, California, USA: Geomorphology, v. 20, p. 177–195, doi:10.1016/S0169-555X(97)00033-0.

Birkeland, P.W., 1964, Pleistocene glaciation of the northern Sierra Nevada north of Lake Tahoe, California: The Journal of Geology, v. 72, p. 810–825, doi:10.1086/627033.

Burke, R.M., and Birkeland, P.W., 1979, The problem of correlation with the Tahoe-Truckee area, Chapter XIV, *in* Friends of the Pleistocene 1979 Pacific Cell Field Trip Guidebook, 22–26 August 1979: San Francisco, California, Friends of the Pleistocene Pacific Cell, p. 114–118.

Bursik, M.I., and Gillespie, A.R., 1993, Late Pleistocene glaciation of Mono Basin, California: Quaternary Research, v. 39, p. 24–35, doi:10.1006/qres.1993.1003.

Bursik, M.I., and Sieh, K., 1989, Range front faulting and volcanism in the Mono Basin, eastern California: Journal of Geophysical Research, v. 94, no. B11, p. 15,587–15,609, doi:10.1029/JB094iB11p15587.

Clark, D.H., and Gillespie, A.R., 1997, Timing and significance of late-glacial and Holocene cirque glaciation in the Sierra Nevada, California: Quaternary International, v. 38/39, p. 21–38, doi:10.1016/S1040-6182(96)00024-9.

Clark, D.H., Gillespie, A.R., Clark, M.M., and Burke, R.M., 2003, Mountain glaciations of the Sierra Nevada, *in* Easterbrook, D.J., ed., Quaternary Geology of the United States, International Association for Quaternary Research, 2003 Field Guide Volume: Reno, Nevada, Desert Research Institute, p.287–311.

Clark, M.M., 1967, Pleistocene Glaciation of the Drainage of the West Walker River, Sierra Nevada, California [Ph.D. dissertation]: Palo Alto, California, Stanford University, 130 p.

Clark, M.M., 1972, Range front faulting: Cause of anomalous relations among moraines of the eastern slope of the Sierra Nevada, California: Geological Society of America Abstracts with Programs, v. 4, p. 137.

Clark, M.M., 1979, Range front faulting: Cause of the difference in height between Mono Basin and Tahoe moraines at Walker Creek, Chapter VI, *in* Friends of the Pleistocene 1979 Pacific Cell Field Trip Guidebook, 22–26 August 1979: Menlo Park, California, Friends of the Pleistocene Pacific Cell, edited by R.M. Burke and P.W. Birkeland, p. 54-57.

Clark, M.M., Harms, K.K., Lienkaemper, J.J., Harwood, D.S., Lajoie, K.R., Matti, J.C., Perkins, J.A., Rymer, M.J., Sarna-Wojcicki, A.M., Sharp, R.V., Sims, J.D., Tinsley, J.C., III, and Ziony, J.I., 1984, Preliminary Slip-Rate Table and Map of Late-Quaternary Faults of California: U.S. Geological Survey Open-File Report 84–106, 12 plates.

Dingler, J., Kent, G.M., Driscoll, N., Babcock, J., Harding, A., Seitz, G., and Goldman, C., 2009, A high-resolution seismic CHIRP investigation of active normal faulting across Lake Tahoe Basin, California-Nevada: Geological Society of America Bulletin, v. 121, no. 7/8, p. 1089–1107, doi:10.1130/B26244.1.

Frankel, K.L., Dolan, J.F., Finkel, R.C., Owen, L.A., and Hoeft, J.S., 2007, Spatial variations in slip rate along the Death Valley–Fish Lake Valley fault system determined from LiDAR topographic data and cosmogenic ^{10}Be geochronology: Geophysical Research Letters, v. 34, p. L18303, doi:10.1029/2007GL030549.

Fraser, G.D., Witkind, I.J., and Nelson, W.H., 1964, The Hebgen Lake, Montana, earthquake of August 17, 1959: A geological interpretation of the epicentral area—the dual-basin concept: U.S. Geological Survey Professional Paper 435, p. 99–106.

Gilbert, G.K., 1890, Lake Bonneville: U.S. Geological Survey Monograph 1, 438 p.

Gillespie, A.R., 1984, Evidence for both Wisconsin and Illinoian ages for the Tahoe glaciation, Sierra Nevada, California: Geological Society of America Abstracts with Programs, v. 16, no. 6, p. 519.

Gillespie, A.R., 1991, Testing a new climatic interpretation for the Tahoe glaciation: Bishop, California, White Mountain Research Station Symposium, v. 3, p. 383–398.

Gillespie, A.R., Huneke, J.C., and Wasserburg, G.J., 1984, Eruption age of an ~100,000-year-old basalt from ^{40}Ar-^{39}Ar analysis of partially degassed xenoliths: Journal of Geophysical Research, v. 89, no. B2, p. 1033–1048, doi:10.1029/JB089iB02p01033.

Hardy, S., and McClay, K., 1999, Kinematic modeling of extensional fault-propagation folding: Journal of Structural Geology, v. 21, p. 695–702, doi:10.1016/S0191-8141(99)00072-3.

Harris, R.A., and Day, S.M., 1999, Dynamic 3D simulations of earthquakes on en echelon faults: Geophysical Research Letters, v. 26, no. 14, p. 2089–2092, doi:10.1029/1999GL900377.

Haugerud, R.A., Harding, D.J., Johnson, S.Y., Harles, J.L., and Weaver, C.S., 2003, High-resolution Lidar topography of the Puget Lowland, Washington—A bonanza for earth science: GSA Today, v. 13, no. 6, p. 4–10, doi:10.1130/1052-5173(2003)13<0004:HLTOTP>2.0.CO;2.

Hawkins, F.F., LaForge, R., and Hansen, R.A., 1986, Seismotectonic Study of the Truckee/Lake Tahoe Area, Northeastern Sierra Nevada, California: U.S. Bureau of Reclamation Seismotectonic Report 85–4, 210 p.

Howard, K.A., and John, B.E., 1997, Fault related folding during extension: Plunging basement-cored folds in the Basin and Range: Geology, v. 25, p. 223–226, doi:10.1130/0091-7613(1997)025<0223:FRFDEP>2.3.CO;2.

Howle, J.F., 2000, The Lake Tahoe basin (LTB), Nevada and California: Meeks Bay right lateral moraines and implications to late Pleistocene glaciations, Lake Tahoe elevations, neotectonics, and fault geometry: Geological Society of America Abstracts with Programs, v. 32, no. 7, p. 244.

Hudnut, K.W., Borsa, A., Glennie, C., and Minster, J.B., 2002, High-resolution topography along surface rupture of the 16 October 1999 Hector Mine, California, earthquake (M_w 7.1) from airborne laser swath mapping: Bulletin of the Seismological Society of America, v. 92, no. 4, p. 1570–1576, doi:10.1785/0120000934.

Hunter, L.E., Howle, J.F., Rose, R.S., and Bawden, G.W., 2011, LiDAR assisted identification of an active fault near Truckee, California: Bulletin of the Seismological Society of America, v. 101, no. 3, p. 1162–1181, doi:10.1785/0120090261.

James, L.A., Harbor, J., Fabel, D., Dahms, D., and Elmore, D., 2002, Late Pleistocene glaciations in the northwestern Sierra Nevada, California: Quaternary Research, v. 57, p. 409–419, doi:10.1006/qres.2002.2335.

Kelson, K.I., Hitchcock, C.S., Zeeb, R.B., Lettis, W.R., and Page, W.D., 1995, Displacement of late Pleistocene glacial moraines by the Almanor fault, Plumas County, CA, *in* Friends of the Pleistocene 1995 Pacific Cell Field Trip Guidebook: San Francisco, California, Friends of the Pleistocene Pacific Cell, p. 1-10, 9 figures.

Kent, G.M., Babcock, J.M., Driscoll, N.W., Harding, A.J., Dingler, J.A., Seitz, G.G., Gardner, J.V., Mayer, L.A., Goldman, C.R., Heyvaert, A.C., Richards, R.C., Karlin, R., Morgan, C.W, Gayes, P.T., and Owen, L.A., 2005, 60 k.y. record of extension across the western boundary of the Basin and Range Province: Estimate of slip rates from offset shoreline terraces and a catastrophic slide beneath Lake Tahoe: Geology, v. 33, no. 5, p. 365–368, doi:10.1130/G21230.1.

Lindgren, W., 1896, Description of the Pyramid Peak Quadrangle, California: U.S. Geological Survey Geologic Atlas Folio 31, 8 p., scale 1:125,000

Lindgren, W., 1897, Description of the Truckee Quadrangle, California: U.S. Geological Survey Geologic Atlas Folio 39, 8 p., scale 1:125,000.

McAllister, J.F., 1936, Glacial History of an Area near Lake Tahoe [M.A. thesis]: Stanford, California, Stanford University, 78 p.

McCalpin, J.P., ed., 1996, Paleoseismology: San Diego, California, Academic Press, 588 p.

McCaughey, J.W., 2003, Pleistocene Glaciation of the Southwest Tahoe Basin, Sierra Nevada, CA [M.S. thesis]: Reno, Nevada, University of Nevada–Reno, 179 p.

Oskin, M.E., Le, K., and Strane, M.D., 2007, Quantifying fault-zone activity in arid environments with high-resolution topography: Geophysical Research Letters, v. 34, p. L23S05, doi:10.1029/2007GL031295.

Phillips, F.M., Zreda, M.G., Smith, S.S., Elmore, D., Kubik, P.W., and Sharma, P., 1990, Cosmogenic chlorine-36 chronology for glacial deposits at Bloody Canyon, eastern Sierra Nevada: Science, v. 248, p. 1529–1532, doi:10.1126/science.248.4962.1529.

Phillips, F.M., Zreda, M.G., Benson, L.V., Plummer, M.A., Elmore, D., and Sharma, P., 1996, Chronology for fluctuations in late Pleistocene Sierra Nevada glaciers

and lakes: Science, v. 274, p. 749–751, doi:10.1126/science.274.5288.749.

Phillips, F.M., Zreda, M.G., Plummer, M.A., Elmore, D., and Clark, D.H., 2009, Glacial geology and chronology of Bishop Creek and vicinity, eastern Sierra Nevada, California: Geological Society of America Bulletin, v. 121, no. 7/8, p. 1013–1033, doi:10.1130/B26271.1.

Prentice, C.S., Crosby, C.J., Whitehill, C.S., Arrowsmith, J.R., and Furlong, K.P., 2009, Illuminating Northern California's active faults: Eos (Transactions, American Geophysical Union), v. 90, no. 7, p. 55–56, doi:10.1029/2009EO070002.

Putkonen, J., and Swanson, T., 2003, Accuracy of cosmogenic ages for moraines: Quaternary Research, v. 59, p. 255–261, doi:10.1016/S0033-5894(03)00006-1.

Russell, I.C., 1885, Geological History of Lake Lahontan: A Quaternary Lake of Northwestern Nevada: U.S. Geological Survey Monograph XI, 283 p.

Schweickert, R.A., Lahren, M.M., Karlin, R., Smith, K., and Howle, J.F., 2000, Preliminary Map of Active Faults of the Lake Tahoe Basin, California and Nevada: Nevada Bureau of Mines and Geology Open-File Report 2000–4, scale 1:62,500.

Schweickert, R.A., Lahren, M.M., Smith, K.D., Howle, J.F., and Ichinose, G., 2004, Transtensional deformation in the Lake Tahoe region, California and Nevada, USA: Tectonophysics, v. 392, p. 303–323, doi:10.1016/j.tecto.2004.04.019.

Shackleton, N.J., and Opdyke, N.D., 1976, Oxygen-isotope and paleomagnetic stratigraphy of Pacific core V28–239 late Pliocene to latest Pleistocene: Geological Society of America Bulletin, v. 145, p. 449–464.

Slemmons, D.B., 1957, Geological effects of the Dixie Valley–Fairview Peak, Nevada, earthquakes of December 16, 1954: Bulletin of the Seismological Society of America, v. 47, p. 353–375.

Smith, K.D., von Seggern, D., Blewitt, G., Preston, L., Anderson, J.G., Wernicke, B.P., and Davis, J.L., 2004, Evidence for deep magma injection beneath Lake Tahoe, Nevada–California: Science, v. 305, p. 1277–1280, doi:10.1126/science.1101304.

Swan, F.H., Schwartz, D.P., and Cluff, L.S., 1980, Recurrence of moderate to large magnitude earthquakes produced by surface faulting on the Wasatch fault zone, Utah: Bulletin of the Seismological Society of America, v. 70, p. 1431–1462.

UCERF2, 2007, Uniform California Earthquake Rupture Forecast version 2, produced by the Working Group on California Earthquake Probabilities: http://pubs.usgs.gov/of/2007/1437/ (see Appendix A for a listing of UCERF2 faults) (accessed May 18, 2011).

Wahrhaftig, C., and Curtis, G.H., 1965, Tahoe City to Hope Valley, *in* Morrison, R.B., and Wahrhaftig, C., eds., Guidebook for Field Conference I, Northern Great Basin and California: International Association for Quaternary Research, Lincoln, Nebraska, Nebraska Academy of Sciences, p. 59–71.

Wallace, R.E., 1977, Profiles and ages of young fault scarps, north-central Nevada: Geological Society of America Bulletin, v. 88, p. 1267–1281, doi:10.1130/0016-7606(1977)88<1267:PAAOYF>2.0.CO;2.

Wells, D., and Coppersmith, K.J., 1994, New empirical relationships among magnitude, rupture length, rupture width, rupture area and surface displacement: Bulletin of the Seismological Society of America, v. 84, p. 974–1002.

Wesnousky, S.G., 2006, Predicting the endpoints of earthquake ruptures: Nature, v. 444, p. 358–360, doi:10.1038/nature05275.

Witkind, I.J., 1964, The Hebgen Lake, Montana, earthquake of August 17, 1959. Reactivated faults north of Hebgen Lake: U.S. Geological Survey Professional Paper 435, p. 37–50.

Yount, J., and LaPointe, D.D., 1997, Glaciation, faulting, and volcanism in the southern Lake Tahoe basin, *in* Field Trip Guidebook for the National Association of Geoscience Teachers, Far Western Section, 1997 Fall Conference: Fallon Nevada, Western Nevada Community College, p. II-1–II-22.

Zielke, O., Arrowsmith, J.R., Ludwig, L.G., and Akciz, S.O., 2010, Slip in the 1857 and earlier earthquakes along the Carrizo Plain, San Andreas fault: Science, v. 327, p. 1119–1122, doi:10.1126/science.1182781.

Zreda, M.G., Phillips, F.M., and Elmore, D., 1994, Cosmogenic ^{36}Cl accumulations in unstable landforms. 2. Simulations and measurements on eroding moraines: Water Resources Research, v. 30, p. 3127–3136, doi:10.1029/94WR00760.

Science Editor: A. Hope Jahren
Associate Editor: Alvaro Crosta

Manuscript Received 30 August 2011
Revised Manuscript Received 8 February 2012
Manuscript Accepted 17 February 2012

Printed in the USA